# The Globular Cluster System of the Auriga Simulations

Timo L. R. Halbesma[1]⋆, Robert J. J. Grand[1], Volker Springel[1], Facundo A. Gómez[2,3], Federico Marinacci[4,5], Rüdiger Pakmor[1], Wilma Trick[1], Philipp Busch[1], Simon D. M. White[1]

[1] *Max-Planck-Institut für Astrophysik, Karl-Schwarzschild-Str. 1, 85741 Garching, Germany*
[2] *Instituto de Investigación Multidisciplinar en Ciencia yTecnología, Universidad de La Serena, Raúl Bitrán 1305, La Serena, Chile*
[3] *Departamento de Física y Astronomía, Universidad de La Serena, Av. Juan Cisternas 1200 N, La Serena, Chile*
[4] *Department of Physics, Kavli Institute for Astrophysics and Space Research, MIT, Cambridge, MA 02139, USA*
[5] *Harvard-Smithsonian Center for Astrophysics, 60 Garden Street, Cambridge, MA 02138, USA*

**ABSTRACT**

We investigate whether the galaxy formation model used for the Auriga simulations can produce a realistic globular cluster population at redshift zero. We compare properties of the simulated star particles in the Auriga haloes with catalogues of observations of the Milky Way and Andromeda globular cluster populations available in the literature. We find that the Auriga simulations do produce sufficient mass at radii and metallicities that are typical for the MW GCS, although we observe a varying mass-excess for the different $R_{GC}$-[Fe/H] bins. This implies different values for the combined product of the bound cluster formation efficiency and the globular cluster disruption rate. Furthermore we test whether any of the Auriga galaxies has a metallicity and radial distribution that is consistent with the MW (M31) GCS. For all of the Auriga haloes we reject the null hypothesis that the simulated and observed metallicities are drawn from the same distribution at $\geq 98.32\,\%$ confidence level, for the GCS of the Milky Way as well as that of the Andromeda galaxy. The same holds true for the distribution of galactocentric radius. Overall, the Auriga simulations produce old star particles with higher metallicities than the MW and M31 GCS and at larger radii. The formation efficiency would have to linearly decrease with increasing metallicity for the Auriga GC candidates to be consistent with the MW GCS.

**Key words:** methods: numerical – galaxies: formation – galaxies: star clusters: general.

## 1 INTRODUCTION

Globular clusters (GC)s are omnipresent, bright, old, and amongst the simplest stellar configurations in the Universe. The GC system of the Milky Way (MW) consists of ∼160 GCs, most of which are older than ∼10 Gyr, and the Andromeda galaxy (M31) hosts roughly twice as many GCs with ages $\geq 6$ Gyr. With masses of $10^{4-6}$ M⊙ within typical half-mass radii of a few parsec, the combined stellar light emitted by GCs makes it possible to obtain integrated properties within the Local Group with reasonable certainty, and even allows for observations beyond the Local Group (e.g. Harris 1991). The extensive literature on GCs is summarised in several books and review articles (e.g. Harris 2001; West et al. 2004; Brodie & Strader 2006; Gratton et al. 2012; Kruijssen 2014; Forbes et al. 2018), and recent analyses of the Gaia data shed new light on the chemical- and structural properties, and on the phase-space distribution of the MW GC system (e.g. Gaia Collaboration et al. 2018; Bose et al. 2018; Posti & Helmi 2019; Vasiliev 2019).

Correlations between GC systems and their host galaxies

The natal gas regions in which globular clusters form inherit key characteristics from their parent (proto-)galaxies. GC populations, in turn, will therefore retain a record of these properties and offer unique insight into the detailed chemical and dynamical evolution history of their host galaxies (see Brodie & Strader 2006, for a recent review). In theory, this information should be readily available and easily observable in the low redshift Universe, given that GCs survive nearly a Hubble time of evolution within the violent galactic environments they live in. However, these long and complex evolution histories themselves impose their imprints onto the GCs observables. Thus, a prerequisite to infer galactic histories from studies of GC systems is to understand the subtleties of the GC formation and evolution itself.

The literature offers a wealth of formation channels, most of which can be broadly classified as ex situ, or as in situ scenarios.

In the former picture, GCs form in smaller, more metal-poor progenitors that are accreted in subsequent mergers, as can naturally be expected in the framework of hierarchical galaxy formation (e.g. Searle & Zinn 1978; Peebles 1984), and Rosenblatt et al. 1988; Cen 2001; Bromm & Clarke 2002; Diemand et al. 2005; Moore et al. 2006; Boley et al. 2009; Griffen et al. 2010; Trenti et al. 2015; Kimm et al. 2016; Ricotti et al. 2016; Boylan-Kolchin 2017; Creasey et al. 2019. As for in situ scenarios, Fall & Rees (1985) propose that thermal instabilities in the collapsing proto-galaxy may lead to GC formation, Ashman & Zepf (1992); Muratov & Gnedin (2010); Choksi et al. (2018) suggest that GC formation is triggered by (major) gas-rich galaxy-galaxy mergers and/or interactions, and Kravtsov & Gnedin (2005) envision GCs to form in the cores of supergiant molecular clouds located within gaseous disks of (high-redshift) galaxies.

Another broad distinction between formation mechanisms are models that rely on special conditions in the early Universe, or those that test the hypothesis that GC formation at high redshift is governed by the same physical processes of young massive clusters (see Portegies Zwart et al. 2010, for a review) in the Local Universe, where differences arise as the result of nearly a Hubble time of (dynamical) evolution. This (latter) scenario is extensively tested in the recent E-MOSAICS project (Pfeffer et al. 2018; Kruijssen et al. 2019a), which comprises a suite of cosmological zoom simulations of MW-like galaxies. As for the former category, Recchi et al. (2017) investigate what fraction of (multiple) stellar populations ends up in bound star clusters after their formation in gravitationally unstable expanding supershells, which arise from hypernova explosions of massive pop. III stars. Chiou et al. (2019) speculate in a recent study that GCs may form in supersonically induced gaseous objects at high redshifts, and Madau et al. (2019) propose that high speed collisions leave cooling gas without their DM subhaloes which could form GC populations that can reproduce the observed $N_{GC} - M_{vir}$ correlation (e.g. Burkert & Forbes 2019) with bimodal metallicity distributions and ages consistent with observations.

One important constraint on plausible formation mechanisms comes from observed bimodality in the colour distribution of most galaxies, believed to be indicative of bimodality in the underlying metallicity distribution of GC systems. GCs in the MW can indeed be split up into a metal-rich (red), and a metal-poor (blue) (sub)population. The former group is associated to the galactic disk because it is a flattened, rotating population found at radii smaller than solar. The latter, on the other hand, is more radially extended, more populated (with three times more blue than red GCs), and may be $\leq 1.5$ Gyr older (De Angeli et al. 2005). The exact dividing metallicity slightly differs between authors, e.g. [Fe/H] $= -0.8$ (according to Zinn 1985), or [Fe/H] $= -1.0$ (according to Harris 2001), and may also differ between galaxies (e.g. Zinn 1985; Gebhardt & Kissler-Patig 1999; Larsen et al. 2001; Peng et al. 2006). In contrast, it has long been debated whether the Andromeda GCS metallicity distribution is uni- bi- or multimodal, and Caldwell & Romanowsky (2016) argue that the data favours three groups (split at [Fe/H] $= -0.4$ and $-1.5$) after more accurate age-measurements improved classification of star clusters as globular (or otherwise). Moreover, the Andromeda GCS has $2 - 3$ times as many GCs at large radii, believed to be indicative of a more rich merger history.

The latter is supported by observed similarities between the spatial distribution and chemical signature of the 'blue' GCs and the Galactic stellar halo (Helmi 2008). Moreover, relative age-estimates indicate that the metal-poor subpopulation may be 1.5 Gyr younger than the metal-rich counterpart (De Angeli et al. 2005), provid-

ing further support that the GC population indeed consists of two distinct classes.

People postulate that the frequent mergers that occur during hierarchical build-up of galaxies naturally produce (sub)populations of GCs from enriched gas on tight orbits, if the mass ratios and gas fractions of the mergers are sufficiently high.

Boylan-Kolchin: the blue population could form in high density regions along the cosmic filament before or during the collapse of the proto-galaxy itself. This formation scenario would explain the presence of the oldest GCs with primordial metallicities in the (outer) haloes of galaxies as the GCs are accreted over time. Moreover, the tidal fields experienced by GCs at (outer) halo orbits is significantly lower than by GCs in the inner galaxy, thus such GCs are expected to be long-lived.

An alternative paradigm is that GC formation does not rely on special conditions at high redshifts. Rather, the same physics that governs the formation of young massive clusters (YMCs) in the Local Group can be applied to the high redshift Universe. The observed differences between YMCs and GCs, in this scenario, arise naturally as the result intrinsic GC evolution within galactic tidal fields over a Hubble time. This interesting hypothesis is tested numerically by the E-MOSAICS people.

Forbes & Bridges (2010) collected age-metallicity observations from the literature and found one track with constant age of 12.8 Gyr, and one track with branches towards younger ages. These branches are dominated by GCs associated with the Sagittarius, Canis Major and other accreted dwarf galaxies, ultimately indicating that 27-47 GCs (about one 25% of the MW GCS) have been accreted from six to eight dwarf galaxies. Kruijssen et al. (2019a,b) show that GC simulated age-metallicity space of the E-MOSAICS suite indeed allows for a reconstruction of the merger history of the Milky Way-like galaxies, and conclude that 40% of the MW GCS has been accreted from galaxies with a stellar mass range of $2 \cdot 10^7 - 2 \cdot 10^9$ M$_\odot$, and $6 \pm 1$ are core remnants of accreted dwarfs.

- Special conditions in early Universe?
- Formation in collapsing proto-galaxies (in-situ-ish?)
- Formation as a result of (wet) mergers?
- Formation in satellites that are later accreted?
- No special conditions at high z, but connection between low-z YMC- and high-z GC-formation where differences could result from Hubble time of evolution?
- This means that in order to test formation models against observations, one not only needs needs to model GC formation, but also include the full evolution over their lifetime in a cosmological tidal field.

**Paragraph: ingredients for numerical studies**

- High resolution in the ISM
- Full cosmological evolution

**Paragraph: narrow down to this work**

The star formation model implemented in the Auriga simulations is capable of producing realistic Milky Way-like (spiral disk) galaxies at redshift zero. Therefore the question naturally arises whether or not the Auriga simulations also produce a subset of star particles (GC candidates) which is consistent with the GC system of the Milky Way and/or the Andromeda galaxy (M31). The typical mass scale of globular clusters is comparable to the numerical (mass) resolution of cosmological zoom simulations. The detailed physics of GC formation in the Universe appears in observations as the combined effect of the $10^{3-6}$ M$_\odot$, compared to a mass resolu-

tion of $10^{3-5}$ M$_\odot$ in the Auriga simulations. Globular clusters can therefore serve as an ultimate test to the star formation model that is implemented in the numerical simulations. Moreover, cosmological zoom simulations provide a detailed (formation and merger) history of the simulated galaxies. This is important because theoretical paradigms for globular cluster formation in the literature know two distinct classes of GCs that are separated by their exact formation sites: an in situ versus an accreted population. Cosmological zoom simulations uniquely allow for an investigation into globular cluster formation with a particular focus on the properties of the in situ versus accreted subpopulations.

Paragraph: Paper outline

We summarise the relevant characteristics of the Auriga simulations in section 2, followed by a summary of the observations of the Milky Way (MW) globular cluster system (GCS) in section 3 that we use to compare our simulations to in section 4. We discuss our findings in section 5 to come to our conclusions in section 6.

## 2 THE AURIGA SIMULATIONS

We use the Auriga simulations (Grand et al. 2017, hereafter G17), a suite of high-resolution cosmological zoom simulations of Milky Way-mass selected initial conditions. The simulations are performed with the state-of-the art code AREPO (Springel 2010; Pakmor et al. 2016), that solves the magnetohydrodynamical equations on a moving mesh, and an elaborate galaxy formation model that produces realistic spiral galaxies at redshift $z = 0$.

The interstellar medium is modelled using a sub-grid approach which implements the physical processes most relevant to galaxy formation and evolution. This model was tailored to the AREPO code and calibrated to reproduce key observables of galaxies, such as the history of the cosmic star formation rate density, the stellar mass to halo mass relation, and galaxy luminosity functions.

The sub-grid includes primordial and metal-line cooling with self-shielding corrections. Reionization is completed at redshift six by a time-varying spatially uniform UV background (Faucher-Giguère et al. 2009; Vogelsberger et al. 2013) The interstellar medium is described by an equation of state for a two-phase medium in pressure equilibrium (Springel & Hernquist 2003) with stochastic star formation in thermally unstable gas with a density threshold of $n = 0.13 \text{cm}^{-3}$, and consecutive stellar evolution is accounted for. Stars provide feedback by stellar winds (Marinacci et al. 2014; Grand et al. 2017), and further enrich the ISM with metals from SNIa, SNII, and AGB stars (Vogelsberger et al. 2013). The formation of black holes is modelled which results in feedback from active galactic nuclei (Springel et al. 2005; Marinacci et al. 2014; Grand et al. 2017). Finally, the simulations follow the evolution of a magnetic field of $10^{-14}$ (comoving) G seeded at $z = 127$ (Pakmor & Springel 2013; Pakmor et al. 2014). See G17 for further details of the numerical setup as well as the galaxy formation model.

The Auriga suite has a fiducial resolution level L4, accompanied by the lower (higher) level L5 (L3) that is available for selected initial condition runs. The baryonic mass resolution in order of increasing level is $m_b = [4 \times 10^5, 5 \times 10^4, 6 \times 10^3]$ M$_\odot$ with gravitational softening of collissionless particles $\epsilon = [738, 369, 184]$ pc. The mass resolution of the Auriga simulations is thus close to the characteristic peak mass of the lognormal GC mass distribution of $10^5$ M$_\odot$ (Harris 1991), although the gravitational softening is two orders of magnitudes larger than typical GC radii. High-density gaseous regions are thus not expected to produce surviving stel-

lar clumps (GCs) with masses and radii consistent with GCs because such objects would numerically disperse, even in the highest-resolution runs. On the other hand, we can investigate (statistical) properties of age-selected GC candidates because each star particle represents a single stellar population with a total mass that could be consistent with one globular cluster.

## 3 OBSERVATIONAL DATA

We describe the observations of the MW GCS in Sec. 3.1, and of the Andromeda (M31) GCS in Sec. 3.2

### 3.1 Milky Way

Harris (1996, 2010 edition; hereafter H96e10) provides a catalogue[1] of the Milky Way globular cluster system that contains properties of 157 GCs. The authors initially estimated the size of the MW GCS to be $180 \pm 10$, thus, their catalogue to be $\sim$85% complete. However, an additional 59 GCs have since been discovered by various authors. The total confirmed number of GCs in the MW adds up to 216 with new estimates now anticipating an additional thirty GCs yet to be discovered (e.g. Ryu & Lee 2018, and references therein). We still use data from the Harris catalogue, but caution that it may (only) be 53-72% complete. Specifically, the relevant data fields that we use from H96e10 are the metallicity [Fe/H], the Galactic distance components $X$, $Y$, and $Z$ (in kpc)[2], and absolute magnitude in the V-band $M_V$. We use the latter to calculate mass-estimates by assuming $M_{V,\odot} = 4.83$ and a mass to light ratio $M/L_V = 1.7$ M/L$_\odot$, the mean for MW clusters (McLaughlin & van der Marel 2005).

We supplement the catalogue with age-estimates from isochrone fits to stars near the main-sequence turnoff in 55 GCs (VandenBerg et al. 2013, hereafter V13). The mean value of the age-estimates in this data set is $11.9 \pm 0.1$ Gyr and the dispersion is 0.8 Gyr. Furthermore, only one of the 55 GC age-estimates is below 10 Gyr.

### 3.2 Andromeda

The fifth revision of the revised bologna catalogue (RBC 5, last updated August, 2012) is the latest edition of three decades of systematically collecting integrated properties of the globular cluster system of the Andromeda galaxy (Galleti et al. 2004, and references therein). One contribution to RBC 5 is the work by Caldwell et al. (2011, hereafter C11), subsequently updated by Caldwell & Romanowsky (2016, hereafter CR16).

C11 and CR16 present a uniform set of spectroscopic observations calibrated on the Milky Way GCS of the inner $1.6°$ ($\sim 21$) kpc that is believed to be 94% complete. GCs in the outer stellar halo, up to $R_{\text{proj}} \sim 150$ kpc, are observed in the Pan-Andromeda Archaeological Survey (PAndAS, Huxor et al. 2014, hereafter H14), but see also Veljanoski et al. (2014) and Mackey et al. (2019). H14 presents the discovery of 59 new GCs and publishes updates to RBC 5. The work of H14 is incorporated in the latest public release[3] of the C11

---

[1] See https://www.physics.mcmaster.ca/Fac_Harris/mwgc.dat
[2] In a Sun-centered coordinate system: $X$ points toward Galactic center, $Y$ in direction of Galactic rotation, and $Z$ toward the North Galactic Pole. We calculate the galactocentric radius $R_{\text{GC}} = \sqrt{(X - R_\odot)^2 + Y^2 + Z^2}$, assuming the solar radius $R_\odot = 8$ kpc.
[3] Last revised 23 Sep 2015, see https://www.cfa.harvard.edu/oir/eg/m31clusters/M31_Hectospec.html
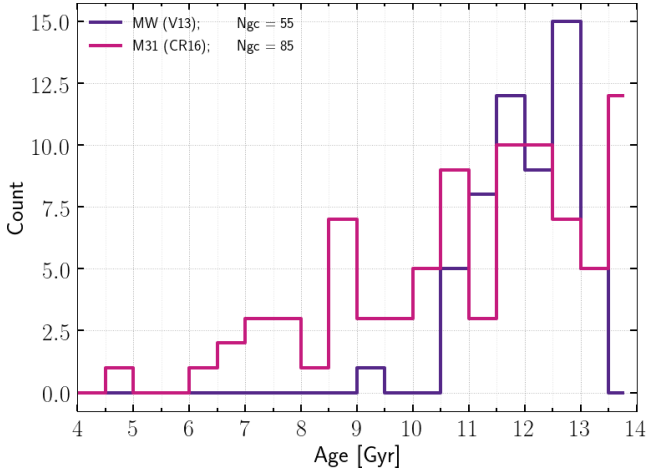
**Figure 1.** Age distribution of 55 GCs in the MW (data from VandenBerg et al. 2013) and 88 GCs in M31 (data from Caldwell & Romanowsky 2016).

dataset, further revised by CR16. It seems that CR16 is the most recent aggregated dataset of M31's GCS that contains properties of interest for our study as it contains GCs in the inner region and in the outer halo. The relevant fields in the CR16 dataset that we use are the age, metallicity, and the mass-estimate[4].

The M31 GCS has a mean age of $11.0 \pm 0.2$ Gyr with a dispersion of 2.2 Gyr, and 24 GCs have age-estimates below 10 Gyr with a minimum age of 4.8 Gyr. We show a histogram of the age-estimates of the 55 MW GCs in V13 and 88 GCs in M31 for which age-estimates are available in CR16, see Figure 1.

### 3.3   Total GC mass in metallicity-radial space

We show the two-dimensional mass-weighted metallicity-radial distribution of the MW (M31) GCS in the top (bottom) panel of Figure 2. Both quantities are readily available in H96e10 (assuming $R_\odot = 8.0$ kpc), but the galactocentric radius of GCs in M31 is not available in CR16. Therefore we follow Wang et al. (2019, Sec. 4.1) to calculate the projected radius $R_{\rm proj}$ from the observed positions, adopting M31's central position from the NASA Extragalactic Database[5] $(\alpha_0, \delta_0) = (0^{\rm h}42^{\rm m}44.35^{\rm s}, +41°16'08.63'')$ and distance $D_{\rm M31} = 778$ kpc (McConnachie et al. 2005; Conn et al. 2012). We calculate $R_{\rm GC}$ as 'average deprojected distance' $R_{\rm GC} = R_{\rm proj} \times (4/\pi)$. The observations indicate that no GCs with high metallicities are to be expected at large radii (the three bins in the upper right corner, both for MW and M31), and relatively few GCs at large radii in general ($R_{\rm GC} > 30$ kpc; right column: 11 GCs or 7.3% in the MW and 17 or 4.6% in M31). We compare these observations to the Auriga simulations later on in Sec. 4.3.

## 4   RESULTS

We define GC candidates in the Auriga simulations as all star particles older than 10 Gyr based on the age distribution of the MW GCS (Figure 1), and following the analysis of Renaud et al. (2017).

Trough out our analysis we compare the distributions of three
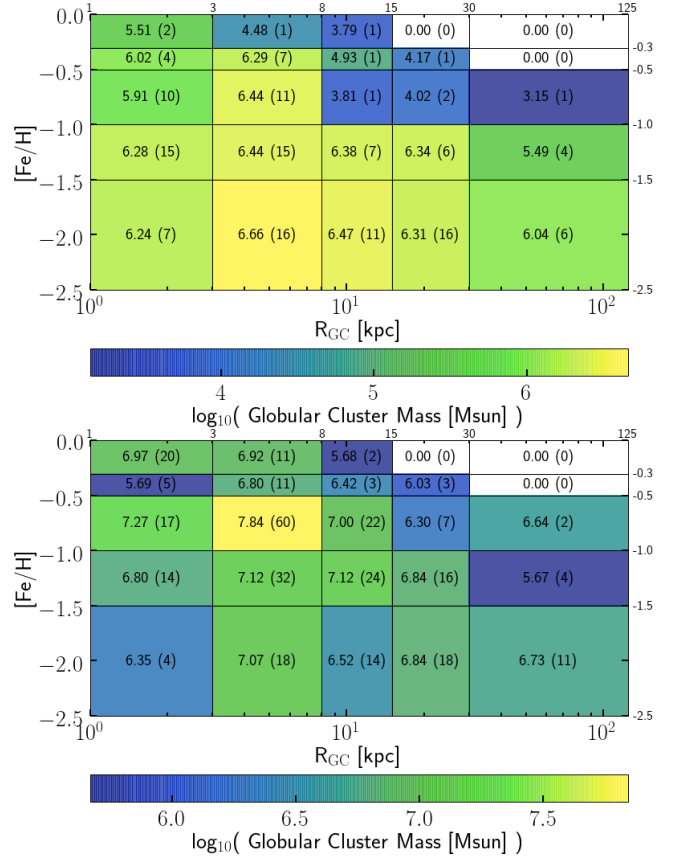
**Figure 2.** *Top*: Mass-weighted $R_{\rm GC}$-[Fe/H] distribution of 151 GCs in the MW (data from Harris 1996, 2010 ed.), which is 98.6 (92.2) % of the total mass (clusters) of the MW GCS in the Harris catalog. *Bottom*: Same for M31, showing 366 GCs and 88.4 (83.9) % of the total mass (clusters) in CR16 (data from Caldwell & Romanowsky 2016). Note that the range of the colourmap differs in both figures.

subsets of star particles: *old stars* (age > 10 Gyr, or GC candidates), *old insitu* stars (defined as those bound to the most-massive halo/subhalo in the first snapshot that the particle was recorded), and *old accreted* star particles (those that have formed ex-situ and are bound to the most-massive halo/subhalo at $z = 0$). For comparison we also include the results for *all stars* (when no additional selection criterion is applied to the star particles). We consider the metallicity distribution in Sec. 4.1, the distribution of galactocentric radii in Sec. 4.2, and the combination of both in Sec. 4.3.

### 4.1   Metallicity distribution

We investigate whether the star formation model implemented in Auriga produces metallicity distributions consistent with the MW (M31) GC system, and whether the subgrid generates sufficient total mass at metallicities typical for the MW (M31) GCS.
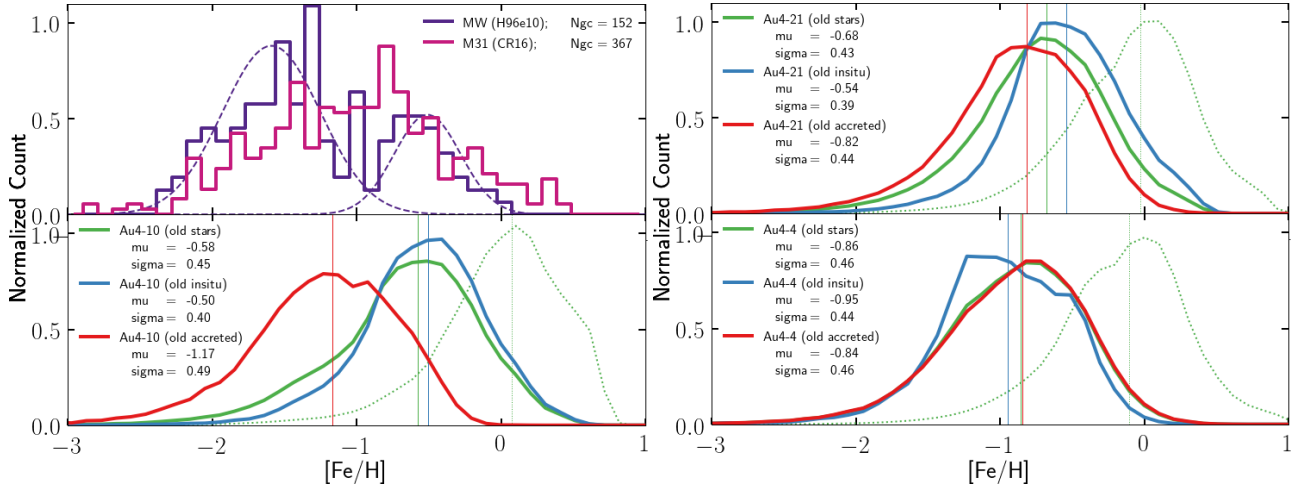
Figure 3 shows the normalized metallicity distribution of Au4-10[6] and Au4-21, showing the GC candidates in green. The
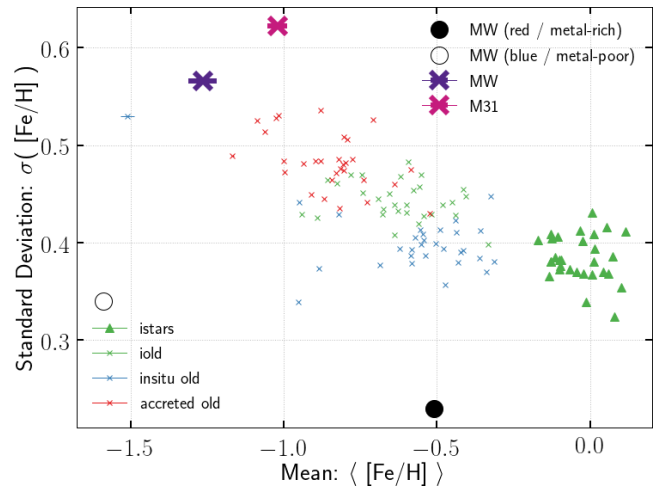
**Figure 3.** *Left:* Metallicity distribution of Au4-10 (bottom panel). We show the GG candicates in green. We split the GC candidates into two subpopulations, those that have formed insitu (blue), and those that have been accreted (red). The dotted green line shows all star particles. The solid purple (magenta) line in the top panel shows the GC system of the MW (M31). *Right:* Au4-4 (bottom), and Au4-21 (top).

accreted GC candidates are shown in red, and the insitu subpopulation in blue. The top panels show the MW (M31) GC system in purple (magenta). We overplot a double Gaussian for the MW GCS (the purple dashed lines), adopting literature values of the mean $\mu$ and standard deviation $\sigma$ of the metal-rich and metal-poor populations (Harris 2001, p. 38).

We find that the age cut lowers the mean metallicity from 0.0 to $-0.6$. Furthermore, the old accreted stars generally have lower metallicities than the old insitu stars. The difference between the mean metallicity of the old insitu and old accreted stars for the majority of the simulations is ~0.3 (e.g. Au4-21), and ~0.5 dex for Au4-10, Au4-16, Au4-17, Au4-18 and Au4-22. This trend is only reversed for Au4-1 and Au4-4, for which the old insitu population has a lower mean metallicity instead. For Au4-1 we find $\mu = -1.51$ (-0.74) for the old insitu (accreted), but the former consists of only 1019 particles (1.3% of all GC candidates, and with a total mass of $5e7\,M_\odot$) thus we believe our classification of insitu is flawed for this halo due to misclassification of the primary halo in the merger tree by subfind. For Au4-4, 10.8 % of the GC candidates is classified as insitu (compared to insitu fractions of $40-80\%$ for other haloes). Overall we find that the simulations produce (sub)populations of GC candidates that are more metal-rich than the MW and M31 GC systems. Moreover, none of the simulations has a population of GC candidates with a bimodal metallicity distribution (the green curves).

We show the mean metallicity and standard deviation of all thirty Auriga L4 haloes in Figure 4. The green crosses are to be compared to the purple (magenta) cross, which shows the mean value of all MW (M31) GCs. We test the null hypothesis that MW (M31) and the GC candidates (all, insitu, and accreted) are drawn from the same underlying distribution by calculating the KS test statistic (i.e. six KS tests per simulation). We reject $H_0$ at the 100.00 % confidence level for virtually all subsets of all simulations, both for MW and M31, except when comparing the old accreted stars of Au4-10 to the MW GCS. In this case we still reject $H_0$ with, but with $\leq 98.68$ % confidence. When comparing to the M31 GCS, the 'best' matches are the old accreted subpopulations of Au4-13, Au4-15, and Au4-17 ($H_0$ rejected with $\leq 99.82$ % confidence, 99.95 %, and 98.32 %). Here we find that the cumulative distributions are more or less similar up to [Fe/H] $-0.5$, above which the simulations yield



**Figure 4.** First vs second central moment of the Auriga L4 metallicity distributions. Each cross (for a given colour) represents one simulation. The green (blue) [red] crosses show the values calculated using the old (old insitu) [old accreted] star particles. Green triangles indicate that all stars were used. The purple (magenta) cross denotes our calculation using all MW (M31) observations (which would be appropriate for a unimodal distribution). The black solid (open) dots indicate the literature values of a bimodal Gaussian fit to the data (values from Ashman & Zepf 1998, p. 38), showing the metal-rich (metal-poor) component of the MW.

higher number counts which drives the KS test statistic over the critical values. This affirms our finding that the simulations produce GC candidates that are more metal-rich than the MW (M31) GCS. The main reason reasons that $H_0$ is rejected with such high confidence are under-production of old stars with [Fe/H] $\leq$ -1.5, and over-production of stars with [Fe/H]$\geq$ -0.5.

In addition, we show the metal-rich (metal-poor) population of the MW GCS using a solid (open) dot. The mean metallicities of the old insitu populations appear roughly consistent with that of the metal-rich population of the MW, but the simulations show larger dispersions. We are uncertain whether definitive consensus is reached concerning uni- or bimodality in the [Fe/H] distribution of

**Figure 5.** Mass-weighted metallicity distribution of star particles in the Auriga simulations. We show the median value of all Auriga haloes for all stars (green dotted) and globular cluster candidates (i.e. stars with age > 10 Gyr; green solid). The latter sub set is further split up between stars that formed in-situ (blue solid), and those that were accreted (red solid). Shaded regions indicate the $1\sigma$ interval. The MW (M31) GCS is shown in purple (magenta). The middle (bottom) panel shows the ratio of the simulated mass to the mass in the MW (M31) GCS.

M31, but CR16 argues that the data, after removal of younger objects due to improved age classification, leans towards unimodality. Therefore we do not show two data points for the M31 GCS.

We now turn to the total mass in GC candidates produced by the Auriga simulations. We show the median (coloured lines) for all thirty Auriga L4 haloes with the $1\sigma$ interval around it (shaded regions, which shows the scatter between runs that have different initial conditions, thus, have unique merger histories). We chose to aggregate the data to indicate a general trend that we find when the GC candidates are split up according to birth location, rather than selecting typical examples of individual galaxies. Figure 5 shows the mass-weighted metallicity distribution of all Auriga L4 galaxies. Once again we notice that the peak metallicity shifts down from 0 to −0.5 for old stars (green solid) compared to all stars (green dotted), and we learn that the mass at the peak lowers by roughly one dex. The mass budget of the old stars is dominated by the old insitu population (blue solid) below [Fe/H] = −1, and by the old accreted stars (red solid) above this value. We show the MW (M31) GCS in purple (magenta) and we show the ratio of the simulated to the observed profiles in the middle (bottom) panel. This mass excess can be thought of the 'mass budget' that the Auriga GC
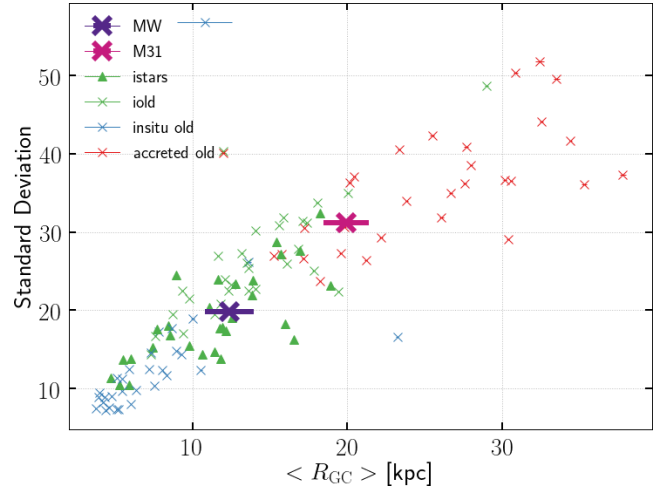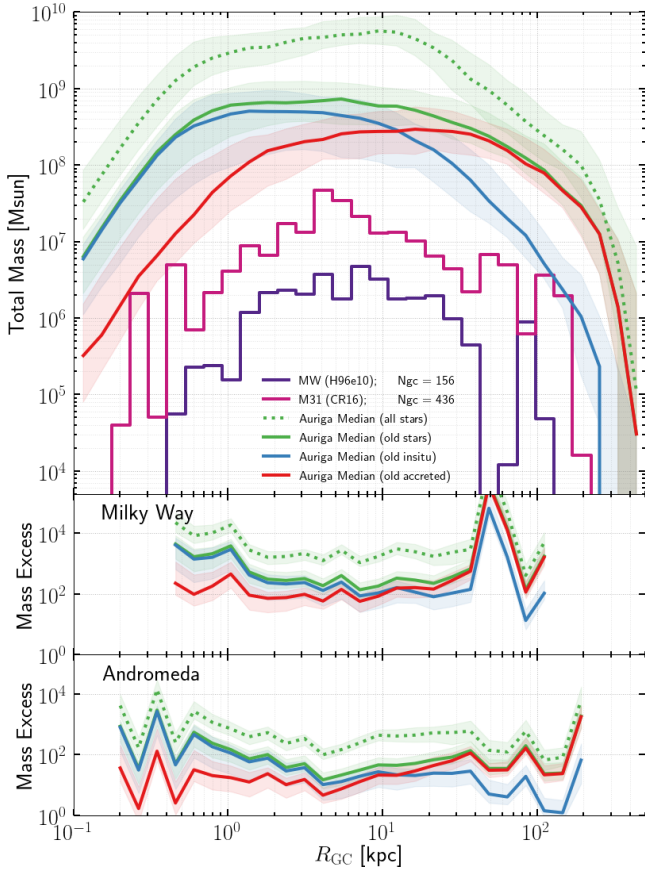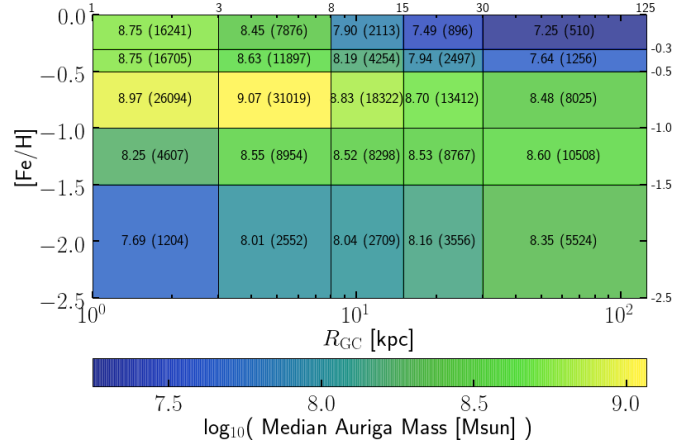


**Figure 6.** Mean and standard deviation of the radial distribution of star particles in each of the thirty Auriga L4 haloes compared to the MW (M31) GCS shown in purple (magenta).

candidates can 'afford to lose' due to a combination of smaller than unity bound cluster formation efficiencies combined with a Hubble time of dynamical evolution, while still producing a GC system with sufficient mass to be consistent with the MW (M31) GCS. The cluster formation efficiency would have to linearly decrease with decreasing metallicity for Auriga GC candidates to produce a population of GC candidates that is consistent with the MW. For the GC candidates in M31 we find a constant mass excess up to −0.9, above which the simulations produce a higher mass excess with increasing metallicity. If dynamical evolution is not expected to more efficiently disrupt GCs of higher metallicity, then we would find that the efficiency to form bound star clusters would have to decrease with increasing metallicity.

## 4.2    Radial distribution

Figure 6 shows the mean and standard deviation of the radial distribution of star particles in all Auriga L4 simulations. We notice that the old insitu populations are much more centrally distributed, whereas the old accreted component has a larger radial extent. Moreover, the dispersion increases with increasing mean value of the radial distribution as may be expected for a non-negative quantity.

Figure 7 shows the mass-weighted radial distribution of the Auriga L4 haloes. We notice a subtle peak around 10 kpc for all star particles that is not present for the GC candidates, indicating that the stellar disc is no longer present when applying the latter selection criterion. Furthermore, we find that the dominant contribution to the total mass in GC candidates changes from those formed insitu to the accreted population around 10 kpc. Again we show the mass excess of the simulations compared to the Milky Way and Andromeda GCS. We find a decreasing mass excess with increasing radius in the range 0.2 to ~5 kpc, followed by an increase attributed to the accreted subpopulation. We further investigate a breakdown of the total mass in Auriga GC candidates into bins of both metallicity and radius in the following section.

**Figure 8.** Mass-weighted [Fe/H]-$R_{GC}$ distribution of all thirty Auriga L4 haloes. Here we consider only the GC candidates (age > 10 Gyr) stars in and color-code by the **median** (values also shown in each bin). The numbers in parenthesis show how many star particles fall within the bin. Note that the range of the colourmap again differs (for improved contrast within the plot).
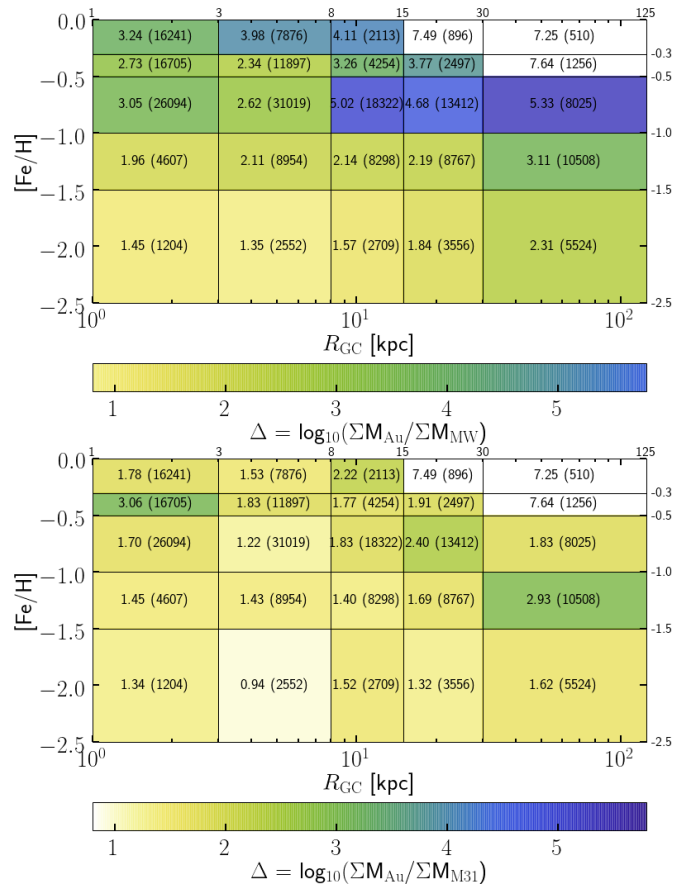


**Figure 9.** The top (bottom) panel shows the logarithm of the ratio of simulated mass to mass in the MW (M31) GCS, i.e. the logarithm of the mass excess. The color-coded values are also shown in each bin. Note that the three bins in the upper right corner are left blank because the observations have zero mass there, and that the numbers indicate how much (median) mass is produced by the simulations in those bins.



**Figure 7.** Mass-weighted radial distribution of star particles in the Auriga simulations. We show the median value of all Auriga haloes for all stars (green dotted) and globular cluster candidates (i.e. stars with age > 10 Gyr; green solid). The latter sub set is further split up between stars that formed in-situ (blue solid), and those that were accreted (red solid). Shaded regions indicate the $1\sigma$ interval. The MW (M31) GCS is shown in purple (magenta). The middle (bottom) panel shows the ratio of the simulated mass to the mass in the MW (M31) GCS.

### 4.3 Total mass in metallicity-radial space

We investigate whether the Auriga simulations still produce sufficient mass when the GC candidates are two-dimensionally binned in [Fe/H] and $R_{GC}$. First we sum the total simulated mass in each bin (for an individual Auriga simulation), then we calculate the median over all thirty Auriga L4 haloes (in each bin, see Figure 8 which can be compared to Figure 2). Finally, we divide these value by the total mass in the MW (M31) GCS to obtain the median mass excess produced by the star formation model implemented in the Auriga simulations. See the top (bottom) panel of Figure 9 for mass excess with respect to the MW (M31) GCS.

## 5 DISCUSSION

### 5.1 Metallicity distribution

We find that the metallicity distributions of GC candidates in the Auriga simulations are more metal-rich than the MW (M31) GCS. Although the (old) star particles represent single stellar populations with a mass (resolution) comparable to the peak of the GCMF, they are in fact statistical tracers of the stellar population of the galaxy as

a whole. Therefore only a (small) fraction of the star particles may represent plausible formation sites of GCs, whereas the majority represent (halo) field stars - the disk component effectively falls outside our selection of star particles due to the age cut. Globular clusters are $\sim 0.5$ dex more metal-poor than spheroid stars observed at the same radius for almost all galaxies (Harris 1991). Our finding that star particles older than 10 Gyr have higher metallicities than the MW (M31) GCS may simply be a reflection thereof.

Ashman & Zepf (1998, p. 234) and Harris (2001, p. 38) quantify the bimodality of the [Fe/H] distribution of the MW GCS, the latter fit a double Gaussian which peaks at [Fe/H] = −1.59 (metal-poor) and −0.51 (metal-rich) and dispersions of 0.34 and 0.23. However, the metallicity distribution of GC candidates in the Auriga simulations is not bimodal, although an offset between the mean values does emerge when further splitting them up according to birth location (accreted or in-situ). The majority of the simulations show an offset in the mean values of roughly 0.3 dex between both subpopulations, while a small number of simulations has an offset of order 0.5 dex. Our finding that the mean values of the old insitu GC candidates are roughly consistent with the metal-rich MW GCs could be interpreted as an indication that this subpopulation may have formed in-situ. However, we also notice that a substantial number of simulations has similar mean values for all GC candidates, and the simulated insitu GC candidates have larger dispersions than the metal-rich GCs. Moreover, the offset between the mean of the metal-rich and metal-poor populations in the MW is 1 dex, a factor $2 - 3$ larger than the offset we find between the insitu and accreted populations. The simulations are not consistent with the picture that all metal-rich GCs formed insitu and that all metal-poor GCs were accreted.

Brodie & Strader (2006) compare the number of metal-poor GCs to the stellar halo mass and find[7] $T^n_{\text{blue}} \sim 100$, while the number of metal-rich GCs compared to the bulge mass yields $T^n_{\text{red}} \sim 5$, and therefore conclude that the formation efficiency of metal-poor GCs is twenty times higher than the metal-rich GCs with respect to field stars.

## 5.2 Radial distribution

The M31 GCS has a factor 2-3 more GCs at large radii compared to the MW GCS, which may indicate that M31 has a richer merger history than the MW. In the Auriga simulations we find that the GC candidates at radii larger than $\sim 20$ kpc are indeed dominated by accreted star particles. However, we select star particles that are bound to the main halo and main subhalo, which means that we include particles up to the virial radius $R_{200}$. The Auriga simulations have no problem populating the stellar halo up to the virial radius, even with our additional age cut. On the other hand, the MW and M31 have fewer GCs at large radii. We expect tidal disruption to be less efficient at larger radii, thus, the formation efficiencies of the accreted GC candidates would have to be lower. Our classification as GC candidates could, for example, be improved by selecting a number of globular clusters based on the $M_{vir} - N_{\text{GC}}$ correlation found by Burkert & Forbes (2019), and taking a virial mass below which none of the star particles is treated as GC candidate.

## 5.3 Star particles are not globular clusters

A major improvement to our classification of star particles as GC candidates could be made by explicitly taking into the formation efficiency of bound star clusters (Kruijssen 2012), which depends on the local ISM properties (density, pressure, sound speed). However, the only information available in post-processing are the properties of the star particles recorded in the first snapshot after formation. We could attempt to obtain the properties of the nearest gas cell, but this would have to be limited to a very narrow time window between the time of formation and the time of the snapshot because the star particle could otherwise be in a completely different location than where it was born initially. Moreover, even if the birth time and snapshot time would coincide, it would not be obvious that the gas cell will yield the correct quantities as the formation of the star itself alters the properties of the gas. We therefore did not further attempt a more sophisticated modeling of the cluster formation efficiency in post-processing.

Furthermore, we compare star particles to present-day globular clusters, thereby ignoring the effects of (dynamical) disruption of globular clusters over nearly a Hubble time. As shown by (Pfeffer et al. 2018), a detailed model of the tidal history of star clusters requires a temporal resolution of order mega year. For the Auriga L4 simulations we have a total of 128 snapshots available over the age of the Universe, thus, far too coarse temporal resolution for meaningful calculations of tidal disruption along the orbit of our GC candidates. Therefore we can only combine these two shortcomings of our analysis into the 'mass excess', which includes the cluster formation efficiency and consecutive globular cluster disruption.

## 6 SUMMARY AND CONCLUSIONS

We investigate GC candidates in the Auriga simulations and draw the following conclusions.

• The star formation model implemented in the Auriga simulations produces metallicity distributions that are more metal-rich the Milky Way and M31 globular cluster systems.

• We reject the null hypothesis $H_0$ that MW (M31) and the GC candidates (all, insitu, and accreted) are drawn from the same underlying distribution for all Auriga L4 galaxies with $\geq 98.68$ % confidence.

• GC candidates in the Auriga simulations may be found out to $R_{200}$, given our selection function of star particles selects all stars bound to the main subhalo in the main halo. The stellar mass is dominated by accreted star particles at radii beyond 20 kpc The GCs in the MW and M31, on the other hand, have a much smaller radial extend.

• The cluster formation efficiency would have to increase with decreasing metallicity for GC candidates in the Auriga simulations to be consistent with the Milky Way GC system, given that we expect dynamical evolution to more strongly affect GC candidates at smaller radii.

• The Auriga simulations are not consistent with the picture that all metal-rich GCs formed insitu and that all metal-poor GCs were accreted.

---

[7] the quantity $T$ is the number of GCs per $10^9$ M$_\odot$ of galaxy stellar mass

# REFERENCES

Ashman K. M., Zepf S. E., 1992, ApJ, 384, 50
Ashman K. M., Zepf S. E., 1998, Globular Cluster Systems
Bose S., Ginsburg I., Loeb A., 2018, ApJ, 859, L13
Brodie J. P., Strader J., 2006, ARA&A, 44, 193
Burkert A., Forbes D., 2019, arXiv e-prints,
Caldwell N., Romanowsky A. J., 2016, ApJ, 824, 42
Caldwell N., Schiavon R., Morrison H., Rose J. A., Harding P., 2011, AJ, 141, 61
Chiou Y. S., Naoz S., Burkhart B., Marinacci F., Vogelsberger M., 2019, arXiv e-prints,
Choksi N., Gnedin O. Y., Li H., 2018, MNRAS, 480, 2343
De Angeli F., Piotto G., Cassisi S., Busso G., Recio-Blanco A., Salaris M., Aparicio A., Rosenberg A., 2005, AJ, 130, 116
Fall S. M., Rees M. J., 1985, ApJ, 298, 18
Faucher-Giguère C.-A., Lidz A., Zaldarriaga M., Hernquist L., 2009, ApJ, 703, 1416
Forbes D. A., Bridges T., 2010, MNRAS, 404, 1203
Forbes D. A., et al., 2018, Proceedings of the Royal Society of London Series A, 474, 20170616
Gaia Collaboration et al., 2018, A&A, 616, A12
Galleti S., Federici L., Bellazzini M., Fusi Pecci F., Macrina S., 2004, A&A, 416, 917
Gebhardt K., Kissler-Patig M., 1999, AJ, 118, 1526
Grand R. J. J., et al., 2017, MNRAS, 467, 179
Gratton R. G., Carretta E., Bragaglia A., 2012, A&ARv, 20, 50
Harris W. E., 1991, ARA&A, 29, 543
Harris W. E., 1996, AJ, 112, 1487
Harris W. E., 2001, Globular Cluster Systems. Springer Berlin Heidelberg, p. 223–408, doi:10.1007/3-540-31634-5_2, https://doi.org/10.1007/3-540-31634-5_2
Helmi A., 2008, A&ARv, 15, 145
Huxor A. P., et al., 2014, MNRAS, 442, 2165
Kravtsov A. V., Gnedin O. Y., 2005, ApJ, 623, 650
Kruijssen J. M. D., 2012, MNRAS, 426, 3008
Kruijssen J. M. D., 2014, Classical and Quantum Gravity, 31, 244006
Kruijssen J. M. D., Pfeffer J. L., Crain R. A., Bastian N., 2019a, MNRAS, 486, 3134
Kruijssen J. M. D., Pfeffer J. L., Reina-Campos M., Crain R. A., Bastian N., 2019b, MNRAS, 486, 3180
Larsen S. S., Brodie J. P., Huchra J. P., Forbes D. A., Grillmair C. J., 2001, AJ, 121, 2974
Mackey A. D., et al., 2019, MNRAS, 484, 1756
Madau P., Lupi A., Diemand J., Burkert A., Lin D. N. C., 2019, arXiv e-prints,
Marinacci F., Pakmor R., Springel V., 2014, MNRAS, 437, 1750
McLaughlin D. E., van der Marel R. P., 2005, ApJS, 161, 304
Muratov A. L., Gnedin O. Y., 2010, ApJ, 718, 1266

Pakmor R., Springel V., 2013, MNRAS, 432, 176
Pakmor R., Marinacci F., Springel V., 2014, ApJ, 783, L20
Pakmor R., Springel V., Bauer A., Mocz P., Munoz D. J., Ohlmann S. T., Schaal K., Zhu C., 2016, MNRAS, 455, 1134
Peebles P. J. E., 1984, ApJ, 277, 470
Peng E. W., et al., 2006, ApJ, 639, 95
Pfeffer J., Kruijssen J. M. D., Crain R. A., Bastian N., 2018, MNRAS, 475, 4309
Portegies Zwart S. F., McMillan S. L. W., Gieles M., 2010, ARA&A, 48, 431
Posti L., Helmi A., 2019, A&A, 621, A56
Recchi S., Wünsch R., Palouš J., Dinnbier F., 2017, Ap&SS, 362, 183
Renaud F., Agertz O., Gieles M., 2017, MNRAS, 465, 3622
Ryu J., Lee M. G., 2018, ApJ, 863, L38
Searle L., Zinn R., 1978, ApJ, 225, 357
Springel V., 2010, MNRAS, 401, 791
Springel V., Hernquist L., 2003, MNRAS, 339, 289
Springel V., Di Matteo T., Hernquist L., 2005, MNRAS, 361, 776
VandenBerg D. A., Brogaard K., Leaman R., Casagrande L., 2013, ApJ, 775, 134
Vasiliev E., 2019, MNRAS, 484, 2832
Veljanoski J., et al., 2014, MNRAS, 442, 2929
Vogelsberger M., Genel S., Sijacki D., Torrey P., Springel V., Hernquist L., 2013, MNRAS, 436, 3031
Wang S., Ma J., Liu J., 2019, arXiv e-prints
West M. J., Côté P., Marzke R. O., Jordán A., 2004, Nature, 427, 31
Zinn R., 1985, ApJ, 293, 424

## APPENDIX A: SCATTER BETWEEN INDIVIDUAL AURIGA HALOES, AND NUMERICAL CONVERGENCE

We check whether the properties of the Auriga globular cluster candidates are well converged between the three different resolution levels used for the Auriga simulations. Here we consider all three Auriga haloes for which simulation runs were performed at all three resolution levels: Au6, Au16, and Au24. Here we can investigate differences between individual haloes.

Figure A1 shows the mass-weighted metallicity distribution, Figure A2 shows the mass-weighted radial distribution, and Figure **??**

This paper has been typeset from a TEX/LATEX file prepared by the author.
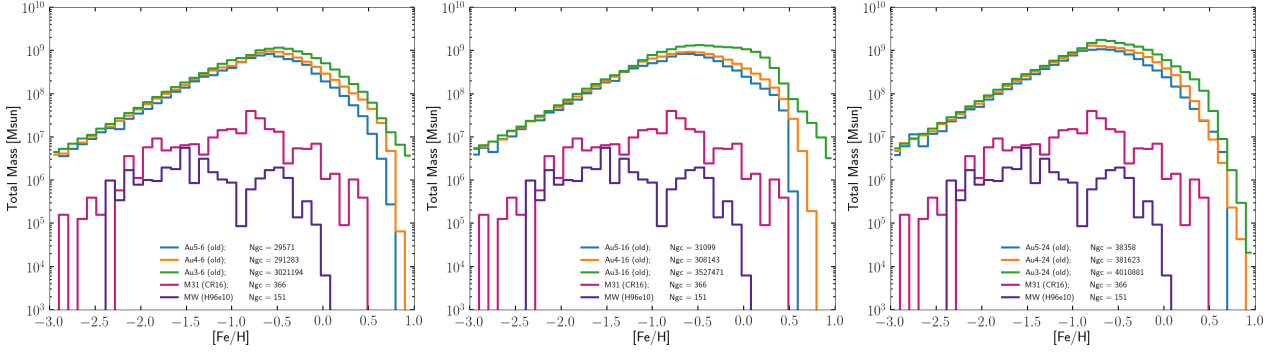
**Figure A1.** Similar to Figure 5, but showing one individual Auriga halo, where colours indicate the resolution level: L3 green, L4 orange, and L5 blue. *Left:* Auriga halo 6. *Mid:* Auriga halo 16. *Right:* Auriga halo 24. For all three haloes we find marginal increases in the mass normalization with increasing resolution level.
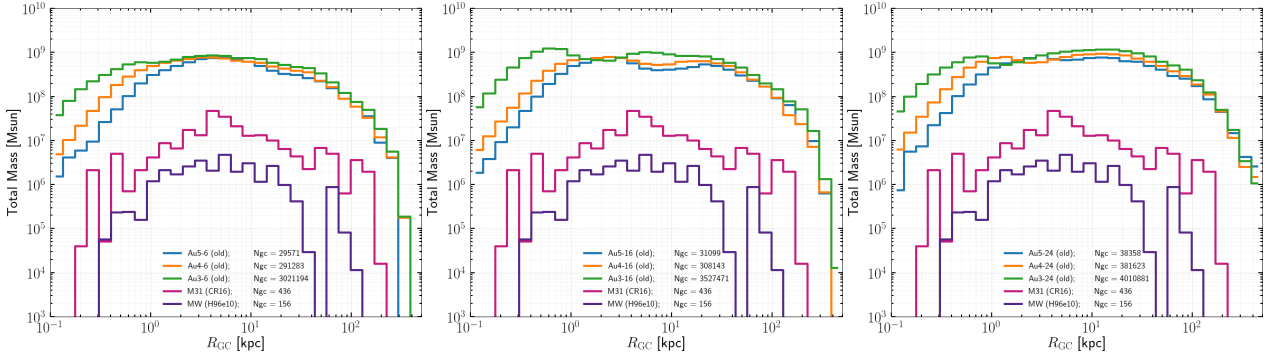


**Figure A2.** Similar to Figure 7, but showing one individual Auriga halo, where colours indicate the resolution level: L3 green, L4 orange, and L5 blue. *Left:* Auriga halo 6. *Mid:* Auriga halo 16. *Right:* Auriga halo 24. For all three haloes we find marginal increases in the mass normalization with increasing resolution level.